LANGMUIR

pubs.acs.org/Langmuir Article

# Surface-Functionalized Terahertz Metamaterial Biosensor Used for the Detection of Exosomes in Patients

Yao Wang, Yuanli Wang,[⊥] Fangrong Hu,* Lizhen Zeng,* Zhencheng Chen, Mingzhu Jiang, Shangjun Lin, Wei Guo, and Dongxia Li

Cite This: *Langmuir* 2022, 38, 3739–3747 Read Online

ACCESS | Metrics & More | Article Recommendations

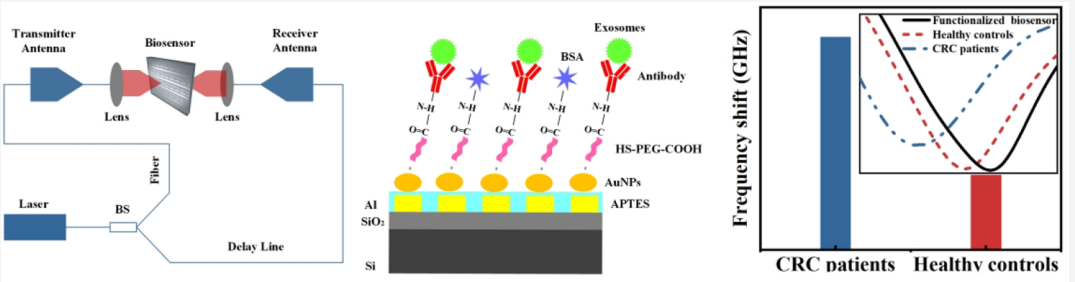


**ABSTRACT:** Owing to their stability in bodily fluids, exosomes have attracted increased attention as colorectal cancer (CRC) biomarkers for early diagnosis. To validate the potential of the plasma exosomes as a novel biomarker for the monitoring of CRC, we demonstrated a terahertz (THz) metamaterials (MMs) biosensor for the detection of exosomes in this work. The biosensor with two resonant frequencies is designed using full wave electromagnetic simulation software based on the finite integration time domain (FITD) method and fabricated by a surface micromachining process. The biosensor surface is first modified using Au nanoparticles (AuNPs), and then, anti-KRAS and anti-CD147, which are specific to the exosomes, are modified on the AuNPs assembled with HS-poly(ethylene glycol)-COOH (HS-PEG-COOH). Exosomes used in the experiment are extracted via the instructions in the exosomes isolation and purification kit and identified by using transmission electron microscopy (TEM), Western blot (WB), and nanoparticle tracking analysis (NTA). The biosensor covered with plasma-derived exosomes of CRC patients has a different resonance frequency shift compared to that with healthy-control-derived exosomes. This study proposes an emerging and quick method for diagnosing the CRC.



## I. INTRODUCTION

Colorectal cancer (CRC) is the third most diagnosed cancer and the second leading cause of cancer deaths in the world.[1] The 5-year survival rate of patients with distant metastasis is extremely poor, approximately 10%.[2] Early detection of CRC improves the 5-year survival rate from 12 to 13% in advanced-stage metastatic disease to 90% in early-stage disease.[3] Therefore, the early detection of CRC metastasis is very important for increasing the survival rate of patients. The gold standard for CRC screening is colonoscopy. However, it is invasive and uncomfortable for patients, and its accuracy depends on the skill level and experience of the operator.[4] Tumor marker levels, such as carcinoembryonic antigen (CEA) levels, can be elevated in CRC, but they are not diagnostic for CRC. The CEA level is also used as a tool to monitor post-treatment follow up and for surveillance.[5] Although labeling techniques, such as fluorescence methods, played a major role in cancer diagnosis, this labeling treatment may cause a cross-reaction between nontargeted molecules, which decreases the specificity of the analysis.[6] These clinical challenges urgently require new biomarkers and methods to effectively diagnose and monitor the prognosis of patients in time. In recent years, cancer markers have received more and more attention, and their important roles in tumorigenesis and tumor development have become more and more obvious. For example, Du et al. investigated ultrasensitive single-molecule techniques for the quantification of 5-methylcytosine (5-mC) and 5-hydroxymethylcytosine (5hmC).[7] Miccio et al. studied the development on liquid biopsy of the label-free detection of "circulating tumor cells" through intelligent labs on chips. Compared to a traditional tissue biopsy that is invasive and does not reveal tumor heterogeneity, a liquid biopsy is noninvasive and provides a real-time reflection of tumor

**Received:** December 10, 2021
**Revised:** March 1, 2022
**Published:** March 17, 2022

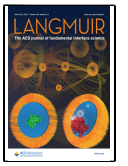





https://doi.org/10.1021/acs.langmuir.1c03286
*Langmuir* 2022, 38, 3739−3747

dynamism and drug sensitivity.[8] Pei et al. designed FeOOH@ZIF-8 composites with an enhanced ionization efficiency and size-exclusion effect for the laser desorption/ionization mass spectrometry (LDI MS)-based metabolic diagnosis of gynecological cancers. The FeOOH@ZIF-8-assisted LDI MS achieved rapid, sensitive, and selective metabolic fingerprints of the native serum without any enrichment or purification.[9] Huang et al. extracted direct metabolic patterns by optimized ferric-particle-assisted laser desorption/ionization mass spectrometry within 1 s using only 50 nL of serum.[10] Su et al. optimized plasmonic alloys to reveal a distinct metabolic phenotype in early gastric cancer.[11] Li et al. demonstrated that MOF/Pt hybrid-assisted LDI MS combined with machine learning analysis of the obtained MFs is a powerful method for aiding CRC diagnosis.[12] Imaging tests are also helpful in diagnosing CRC, including computed tomography (CT), nuclear magnetic resonance (NMR), a roentgenographic (Rtg) examination of the thorax, endorectal ultrasonography (USG), and abdominal USG. However, these methods are efficient only in cases of severe focal lesions or during the middle−late stage.[13] Noninvasive tests including the serum detection of tumor markers (e.g., CEA) and fecal occult blood testing (FOBT) are associated with low sensitivity and specificity, especially in early stages. DNA methylation biomarkers have recently been found to have higher accuracy in CRC detection and an enhanced prediction of the prognosis and chemotherapy response. Other screening methods include colon capsule endoscopy (CCE) and DNA tests, and CCE limitations include the intensive laxative preparation needed and the time required to read every study.[14,15] Compared to traditional biological detection, this study proposes a new method for the rapid diagnosis of CRC, which has unique advantages such as being label-free, nondestructive, highly reproducible, and highly specific.

Exosomes were first discovered by Johnstone in 1987[16] and consist of lipid bilayers, such as cystic structures, with diameters ranging from 40 to 150 nm. Exosomes contain proteins, lipids, RNA, and other substances, which can be received by recipient cells to realize material transport and information transmission between cells. Exosomes are closely related to tumor invasion and metastasis and play an important regulatory role in the occurrence and development of the CRC. In recent years, biomarkers based on exosomes have become a powerful diagnostic tool for CRC. Genetic mutations in key biomarkers are known to predict outcomes and responses to treatment in metastatic CRC. KRAS mutations have been implicated in approximately in nearly 40% CRC cases.[17,18] CRC cell KRAS releases more exosomes, and the protein composition is changed. The transfer of proteins carried by these exosomes to surrounding KRAS wild-type cells will significantly stimulate their growth,[19] which indicates that there are components in the exosomes that can suggest the KRAS mutation of CRC cells. Hence, various investigations have identified it as a clinically prognostic and predictive marker in CRC.[20,21] The research discovered significantly elevated levels of transmembrane protein CD147 exosomes in the plasma of CRC patients.[22] So far, many methods have been developed to analyze tumor-cell-derived exosomes. Traditional methods, such as an enzyme-linked immunosorbent assay (ELISA), WB, and NTA, can be used to detect exosomes. However, these methods are limited to large sample consumption, time-consuming sample preparation, expensive equipment, and low sensitivity. A typical fluorescence detection method is one of the most widely used methods in cell detection. Generally, fluorescence comes from different labels. Fluorescent chemicals can be used to label cellular components. Unlike the proposed MMs biosensors, the cost of fluorescent detection is not cheap, and the detection preparation is complicated because of the irrecoverable consumption of fluorescently labeled antibodies and the steps involved. Another method used for biological measurements is electrochemical measurements. This technique measures the potential difference between two electrodes. However, if the cell is located near the electrodes, then the activity of all of the other cells will generate noise, which may interfere with the measurement. In recent years, some work has also been carried out on new methods of exosome analysis, such as the coordination between the phosphate structure on the exosome membrane and zirconium,[23,24] by means of the steric hindrance effect of exosome nanostructures,[25,26] by enzymatic signal amplification,[27,28] or by using covalent organic framework materials.[29]

Terahertz time domain spectroscopy (TDS) is a cutting-edge technology and has potential applications in biomedical detection[30−32] and substance identification.[33] The photon energy of a THz wave is about 4.1−40 meV, so it will not produce ionizing radiation and chemical damage to biological tissues.[34] In addition, the THz MMs biosensor has been evaluated as a promising biosensor method because of its keen sensitivity and good penetration to biomolecular interactions.[35] The electromagnetic field in the MMs has a strong restrictive effect, which can detect the small changes in biomolecules.[36] Therefore, THz spectroscopy detection technology has been widely used in the label-free nondestructive testing and analysis of biological substances.[37−41]

To validate the potential of the plasma exosome as a novel biomarker for the monitoring of CRC, the current study investigated whether the KRAS mutation and CD147 in the plasma exosomes of patients with CRC could be detected by the THz MMs biosensor. In this study, the THz MMs biosensor with a theoretical sensitivity of 103 GHz/RIU (RIU: refractive index unit) is proposed to detect the reaction between exosomes and antibodies (anti-KRAS and anti-CD147), and the resonance frequency shift produced by plasma exosomes derived from CRC patients is different from that from healthy controls. The FITD method is introduced to design the biosensor, and the surface micromachining process is used to fabricate the biosensor. After surface modification of the biosensor, the proposed THz MMs biosensor can be used to quickly detect plasma exosomes and thus help to diagnose the CRC.

## II. DESIGN, FABRICATION, AND EXPERIMENTAL SECTION

**II.A. Metamaterials Biosensor Design and Fabrication.** The MMs biosensor is simulated with CST Microwave Studio 2019 full-wave electromagnetic simulation software. Figure 1a presents a local schematic of the biosensor with 2 cells × 5 cells. The biosensor has a triple-layer structure. The top layer is made of lossy aluminum with a conductivity of $\sigma = 3.471 \times 10^7$ S/m. The bottom layer is composed of a high-resistance silicon substrate with a dielectric constant of $\varepsilon = 11.9$, and the spacer between the top layer and bottom layer is silicon dioxide with a dielectric constant of 3.75. The periodic array unit is composed of metal wire structures of different sizes. The structural parameters of the unit cell are shown in Figure 1b. The unit size is $W_1 \times W_5 = 56 \times 192$ $\mu$m. $D$ is the width of the gap, $T_1-T_5$ represent the width of the wire, $W_1-W_5$ represent the length of the wire, and $H_1-$


https://doi.org/10.1021/acs.langmuir.1c03286
Langmuir 2022, 38, 3739−3747

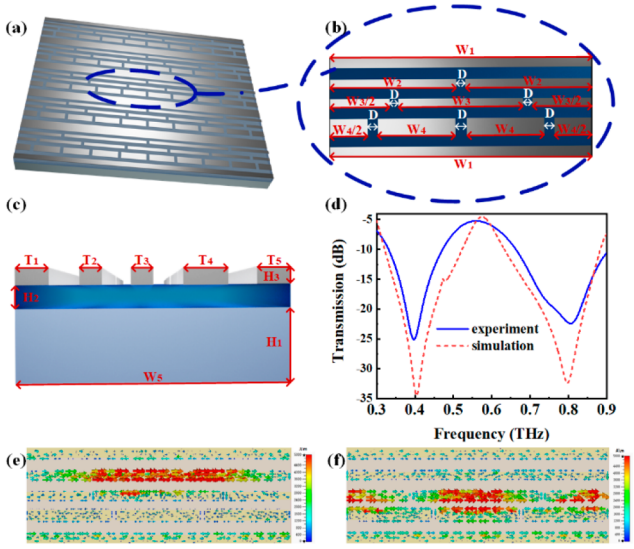


**Figure 1.** (a) Local schematic of the biosensor. (b) Top view. (c) Cross-sectional view. (d) Simulated and experimental transmission spectrum. Surface current diagrams at (e) $f_2$ and (f) $f_2$.

$H_3$ represent the thickness of each layer. Figure 1e,f shows the surface current distribution at low and high resonance frequencies, respectively, and these indicate that they are typical dipole oscillations. Table 1 lists the parameter values.

**Table 1. Structural Parameters of the Unit ($\mu$m)**

| $W_1$ | $W_2$ | $W_3$ | $W_4$ | $W_5$ | $T_1$ | $T_2$ |
|---|---|---|---|---|---|---|
| 192 | 94 | 92 | 60 | 56 | 6 | 4 |
| $T_3$ | $T_4$ | $T_5$ | $D$ | $H_1$ | $H_2$ | $H_3$ |
| 4 | 8 | 6 | 4 | 20 | 0.5 | 0.2 |

To understand the potential resonance mechanism, the transmission spectrum of the THz MMs biosensor is simulated and measured. As shown in Figure 1d, the simulated results at $f_1$ = 0.403 THz and $f_2$ = 0.797 THz are similar to the experimental results except for the strength. The distinctions between the simulated and experimental data are mainly due to errors in fabrication. To study its physical mechanism further, the surface current distributions of the biosensor at $f_1$ = 0.403 THz and $f_2$ = 0.797 THz are monitored.

Meanwhile, to further evaluate the mechanism of detection by the THz MMs biosensor, the FITD method is utilized to simulate the resonance frequency shifts caused by the analyte with a different refractive index and thickness. With a refractive index of $n$ = 2.0, the thickness of the analyte increases from $d$ = 0 to 25 $\mu$m. The corresponding transmission spectra and the resonance frequency shift changing with refractive index are shown in Figure 2a,b, respectively. Figure 2b shows that the resonance frequency shift of the calculated biosensor tends to saturate when the thickness of the analyte exceeds 5 $\mu$m. Therefore, the influence of analyte thickness on the biosensor can be eliminated by using an analyte with a thickness of 20 $\mu$m.

With a 20-$\mu$m-thick analyte, the refractive index of the analyte changes from $n$ = 1.0 to 2.0, the influence of the refractive index on the THz MMs biosensor is demonstrated in Figure 2c, and the corresponding changes in the resonance frequency shift with the refractive index are plotted in Figure 2d. The sensitivity per unit volume ($S$) is defined as the resonance frequency shift of the unit refractive index change for the unit volume sample; that is, $S = \Delta f/\Delta n$, where $\Delta f$ is the resonance frequency shift and $\Delta n$ is the change in the refractive index. Both low and high resonance frequencies are highly sensitive to changes in the microenvironment. The $S$ values at $f_1$ = 0.403 THz and $f_2$ = 0.797 THz are 63 and 103 GHz/RIU, respectively. For the THz MMs biosensor with the resonance frequency of $f_2$, the resonance frequency shift increased more rapidly than for $f_1$, as shown in Figure 2d, indicating a better sensitivity for the microenvironment. Consequently, in the following experiments, we use only $f_2$ to characterize the reaction between the antibody and the exosomes.

The general process of sample processing is as follows: (a) a layer of silicon dioxide film is prepared on the silicon wafer; (b) a layer of photoresist is coated on the silicon dioxide surface using a glue spreader and then baked to dryness; (c) the photoresist is exposed using an ultraviolet exposure system and (d) developed in a developer to form a pattern; (e) after drying, it is used as an electron beam evaporation deposition system for metal deposition; and (f) the photoresist is removed with acetone and (g) diced with a microtome to obtain a biosensor sample. The standard electronic module (SEM) image of the biosensor is shown in Figure 3a.

**II.B. Reagents and Instruments.** Anti-KRAS (101667-T32), anti-HSP60 (101240-T38), and anti-CD147 (10186-R125) were purchased from Beijing Yiqiao Shenzhou Technology Co., Ltd. Gold chloride hydrate, sodium citrate, absolute ethanol, APTEs ((3-aminopropyl)triethoxysilane), HS-PEG-COOH, 1-(3-(dimethylamino)propyl)-3-ethylcarbodiimide hydro (EDC), *N*-hydroxysuccinimide (NHS), and phosphate-buffered saline (PBS, pH = 7.4) were all purchased from Shanghai Aladdin Biochemical Technology Co., Ltd. The plasma exosomes extraction kit was purchased from Umibio Science and Technology Group.

The instrument used in the experiment is an all-fiber THz-TDS system produced by THz Photonics Technology (Tianjin, China) (model TPF15K), with a spectral range of 0.1−3.5 THz. The schematic diagram is shown in Figure 3b.

**II.C. Preparation of AuNPs.** AuNPs are prepared by the general method of reducing chloroauric acid (HAuCl4) with sodium citrate:[42] (a) A 0.01% chloroauric acid solution (100 mL) is poured into a round-bottomed flask and heated to boiling under stirring. (b) A 1% sodium citrate solution (2 mL) is slowly added dropwise to the boiling chloroauric acid solution, keeping the solution in a boiling state, and stirred. It can be observed that the solution changes from colorless to red and finally to wine red. (c) The solution is heated for another 15 min and then allowed to stand and cool to room temperature. (d) The AuNPs solution with a particle size of about 20 nm is obtained and stored away from light at 4 °C.

**II.D. Sample Preparation.** In the present study, 25 plasma samples were provided by the Department of Oncology, The First People's Hospital of Qinzhou, Guangxi province, China. Among them, 18 samples were taken from patients diagnosed with CRC on the basis of imaging and pathological findings (Figure 6l, 1−18), and 7 plasma samples were taken from healthy controls (Figure 6l, 19−25).

**II.E. Exosome Extraction.** Plasma exosomes were extracted according to the instructions in the exosomes isolation and purification kit. The morphology of the exosomes was examined by TEM, and the expression of exosome marker proteins is assessed by WB analysis. The size distribution and concentration of exosomes are determined using NTA. The purified exosomes are stored at −80 °C for subsequent experiments.

## III. RESULTS AND DISCUSSION

**III.A. Isolation and Identification of Exosomes.** Extracted exosomes are found to be 40−150 nm in size and exhibit a round or spindle shape (Figure 4a). The exosome concentration was determined using a bicinchoninic acid (BCA) assay kit (Pierce BCA protein assay kit, Thermo Fisher Scientific), and the exosome was diluted to make the same concentration, 0.2 $\mu$g/$\mu$L. The expression of KRAS and CD147 proteins in the exosomes separated from the plasma samples of patients with CRC is higher than in the healthy controls (Figure 4b). No significant difference is observed in the expression level of exosomes marker HSP60 between patients with CRC and healthy controls (Figure 4b). The NTA


https://doi.org/10.1021/acs.langmuir.1c03286
Langmuir 2022, 38, 3739−3747

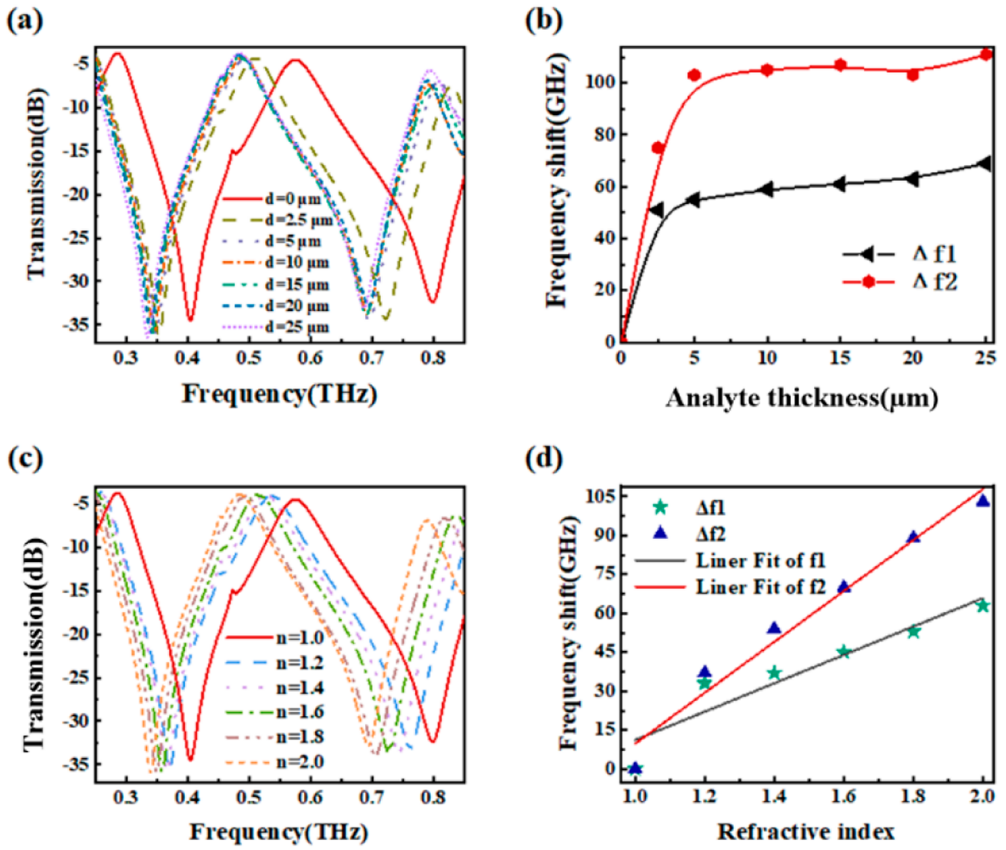


**Figure 2.** (a) Transmission spectra and (b) the resonance frequency shift versus thickness for the analyte with refractive index $n$ = 2.0. (c) Transmission spectra and (d) frequency shift versus refractive index for analyte thickness $d$ = 20 $\mu$m.

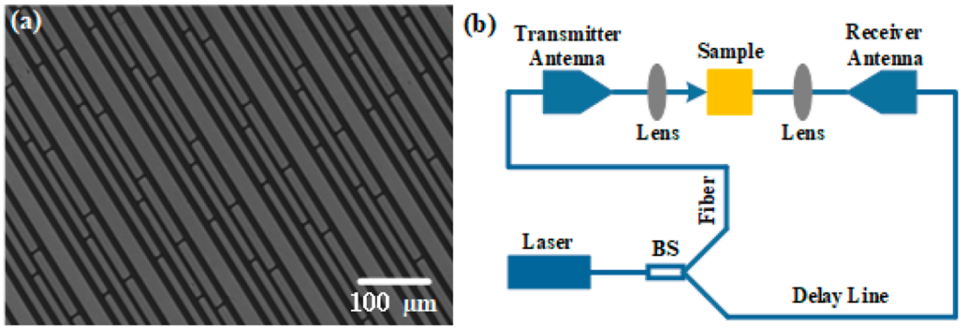


**Figure 3.** (a) SEM image of the biosensor. (b) Schematic diagram of the THz-TDS system.

data also revealed that the number of exosomes in patients with CRC is increased compared to the number in the control group (Figure 4c,d), and the $p$ value is 0.0075. Generally, cancer cells produce and release more exosomes than normal cells, and the molecules contained in tumor-cell-derived exosomes are significantly different than those in normal cells.[43] The results of the current study indicated that plasma exosomes had the potential to be used for KRAS gene mutation detection in patients with CRC.

**III.B. Surface Functionalization of a Biosensor.** To apply the THz MMs biosensor to the analysis of exosome expression in the diagnostics of CRC, anti-KRAS and anti-CD147 are used to functionalize the biosensor. Figure 5 summarizes the major steps in the functionalization process. In Figure 5b, the biosensor is functionalized with APTES, which modified its surface with a layer of amino groups. The interaction between AuNPs and amino groups leads to the strong electrostatic adsorption of nanoparticles on the surface of the biosensor, as shown in Figure 5c. Figure 5d,e shows that HS-PEG-COOH is assembled onto the AuNPs with the Au−S bond, and the carboxyl moiety on the AuNPs is activated using EDC/NHS coupling chemistry. After washing with the PBS solution (0.1 mol/L, pH 7.0) to remove the excess antibody, the possible remaining active sites against nonspecific adsorption are blocked with 0.5% BSA solution, as shown in Figure 5f. Subsequently, the antibody is loaded into the biosensor, as shown in Figure 5g.

**III.C. Detection of Exosomes by an Anti-KRAS-Modified Biosensor.** As shown in Figure 6a, $T_1$−$T_{10}$ is the number of times the cleaned sensor is randomly selected, and the average value is taken as the data of the cleaned biosensor. The accuracy of the terahertz system is 3 GHz. Comparing the


https://doi.org/10.1021/acs.langmuir.1c03286
Langmuir 2022, 38, 3739−3747

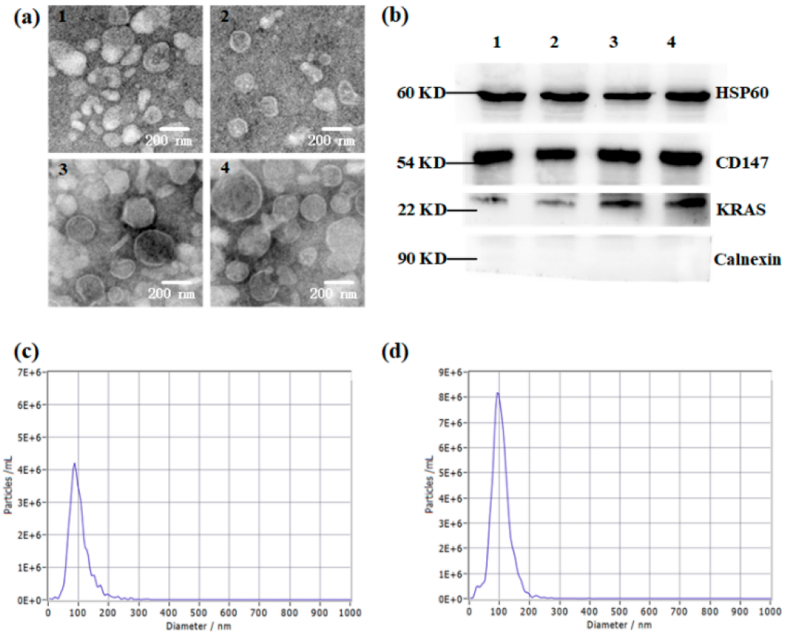


**Figure 4.** Isolation and identification of exosomes from plasma samples of CRC patients. (a) The exosomes are separated from the supernatant according to the instructions in the exosomes extraction kit, and representative images of healthy controls (1 and 2) and CRC patients (3 and 4) are captured via TEM. Scale bar, 200 nm. (b) Purified exosome protein is concentrated and then analyzed using WB. The levels of KRAS protein, CD147 protein, and the exosome marker (HSP60) are determined using WB and calnexin, which is used as an exosome marker negative control. The size distribution of exosomes from plasma samples of (c) a healthy control and (d) a CRC patient is measured with NTA.

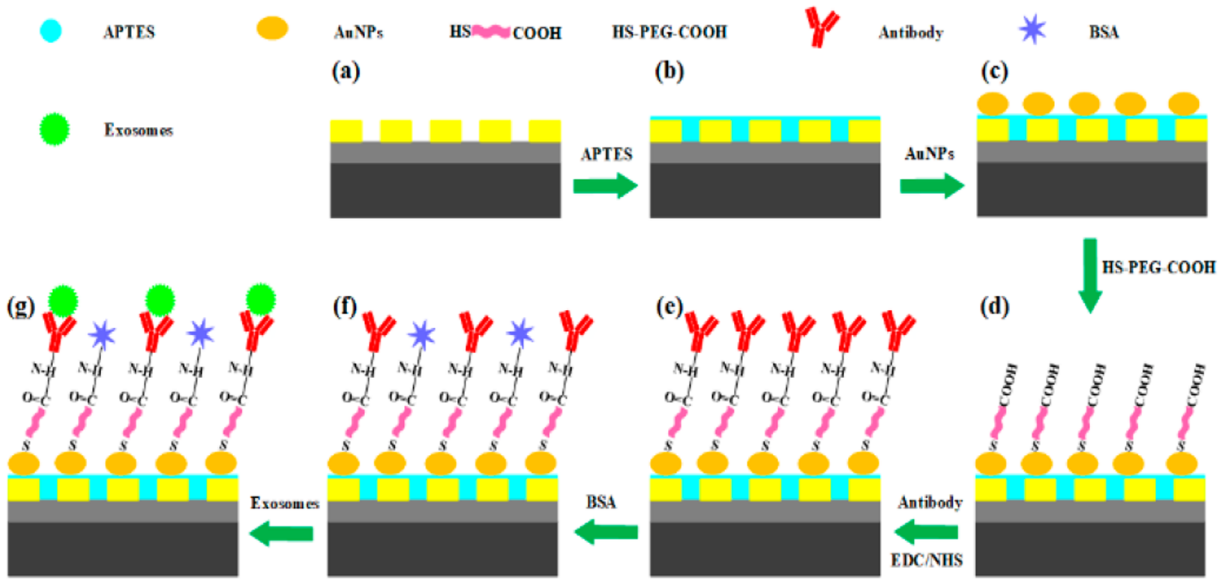


**Figure 5.** Flowchart for the surface functionalization of the biosensor.

spectra of the biosensor before modification and after cleaning, there is almost no difference, which proves that the biosensor has good repeatability.

By comparing the detection results of the bare silicon wafer, the bare biosensor, and the anti-KRAS-modified biosensor before and after adding exosome samples, the detection performance of the modified THz MMs biosensor is verified. As shown in Figure 6c, the exosomes samples are directly added to the bare silicon wafer for comparison. It is found that there is almost no difference in the corresponding transmission spectral lines, so the silicon wafer did not have the ability to identify. By comparing the transmission spectra before and after adding exosomes samples to the bare biosensor, it is observed that the resonance frequency shift of the bare biosensor has a red shift of 62 GHz, indicating that the biosensor has recognition ability. After exosomes are added to the anti-KRAS-modified biosensor, it is observed that resonance peak $f_2$ is significantly red-shifted by 73 GHz, indicating that this modification method is effective and can be used to analyze exosomes from CRC patients.

Before verifying the detection sensitivity, it is very important to determine the specificity and repeatability of the detection. The anti-KRAS-modified biosensor is added to Afp, Ca125, Ca199, Her2, and exosomes samples (samples 14 and 3 reach


https://doi.org/10.1021/acs.langmuir.1c03286
Langmuir 2022, 38, 3739−3747

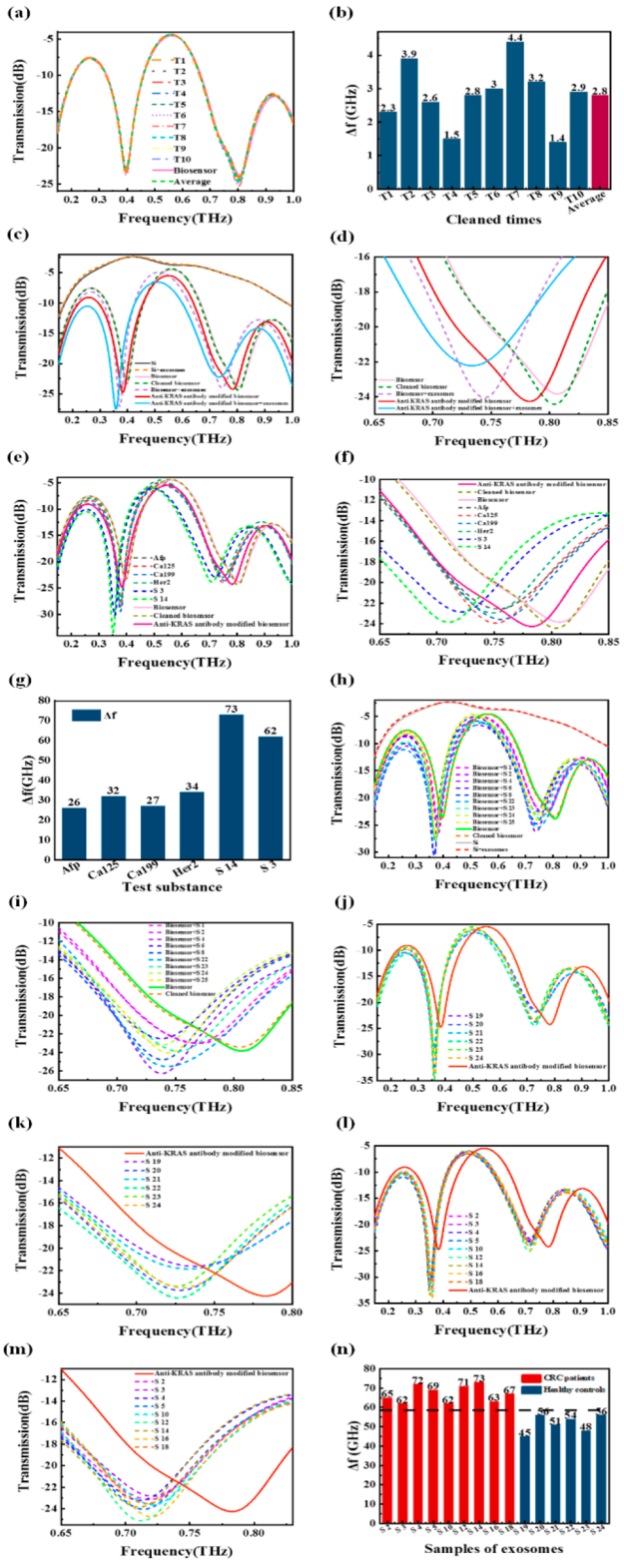


**Figure 6.** (a) Transmission spectra before and after cleaning the sensor. (b) Resonance frequency shift histogram before and after cleaning the sensor. (c) Transmittance spectra of silicon wafers, a biosensor, and the anti-KRAS-modified biosensor before and after the addition of exosome samples and after cleaning the biosensor. (d) Magnified view of panel c. (e) Transmission spectrum of the anti-KRAS-modified biosensor after dropping different test substances. (f) Magnified view of panel e. (g) Histogram of the resonance frequency shift with six test substances. (h) Transmittance spectra before and after different exosomes samples are dropped directly on the surface of the biosensor and after cleaning. (i) Magnified view of panel h. (j) Transmission spectra of exome samples from patients with CRC and (l) healthy controls. (k) Magnified view of panel j. (m) Magnified view of panel l. (n) Frequency offset histogram (KRAS mutation) of CRC and healthy controls.

the maximum and minimum values of the resonance frequency shift of exosomes) to verify its specificity. It can be seen from Figure 6g that after adding six different detection substances to the anti-KRAS-modified biosensor, resonance peak $f_2$ of the biosensor transmission spectrum is red-shifted by 26, 32, 27, 34, 73, and 62 GHz. The smallest resonance frequency shift of the exosome sample is 45% higher than that of the other four detection substances, and the largest resonance frequency shift of the exosome sample is 53% higher than that of the other four detection substances. In comparison experiments with other proteins (such as Ca125, Ca199, and Her2), the $p$ value is 0.0047 after statistical analysis. Comparing the detection results of two exosome samples with those of other substances shows that the anti-KRAS-modified biosensor has high specificity, and our method can specifically recognize exosomes and can potentially be used to analyze exosome samples from healthy controls and patients with CRC. As shown in Figure 6h, the bare biosensor is directly used to measure the THz transmission spectrum of the exosomes. The results show that the THz transmission spectra of all of the samples have a resonance frequency shift, so the bare biosensor cannot distinguish between the exosomes of patients with CRC and healthy controls.

The THz transmission spectrum of exosomes is measured using the anti-KRAS-modified biosensor, as shown in Figure 6n. The detected exosome samples are from CRC patients with the KRAS mutation and healthy controls. According to the experimental data, it is observed that the resonance peaks of patients with CRC are less than 0.725 THz, and the resonance peaks of healthy controls are greater than 0.725 THz. After calculating the resonance frequency shift, it is found that the resonance frequency shift of patients is more than 59 GHz and that of healthy controls is less than 59 GHz. This shows that our method can potentially be used to analyze the exosomes of CRC patients with the KRAS mutation and healthy controls. Six groups of data were selected from the healthy group and the patient group for statistical analysis. The $p$ value is 0.0002, and the SD value is 4.6224.

**III.D. Detection of Exosomes by an Anti-CD147-Modified Biosensor.** First, the detection performance of the proposed anti-CD147 modified biosensor is tested and compared with that of the unmodified biosensor. The experimental transmission spectrum results before and after modification are shown in Figure 7a. The resonance peak of the unmodified biosensor has a resonance absorption dip at 0.806 THz, and the resonance frequency of the modified biosensor is located at 0.762 THz. The resonance frequency difference between the two devices is caused by the modification used for the biosensor. The test results showed that the biosensor without the anti-CD147 modification could not distinguish between exosomes samples from CRC patients and healthy controls. Comparing the spectrum of the biosensor before modification and after cleaning, there is almost no difference, which proves that the biosensor has good


https://doi.org/10.1021/acs.langmuir.1c03286
Langmuir 2022, 38, 3739−3747

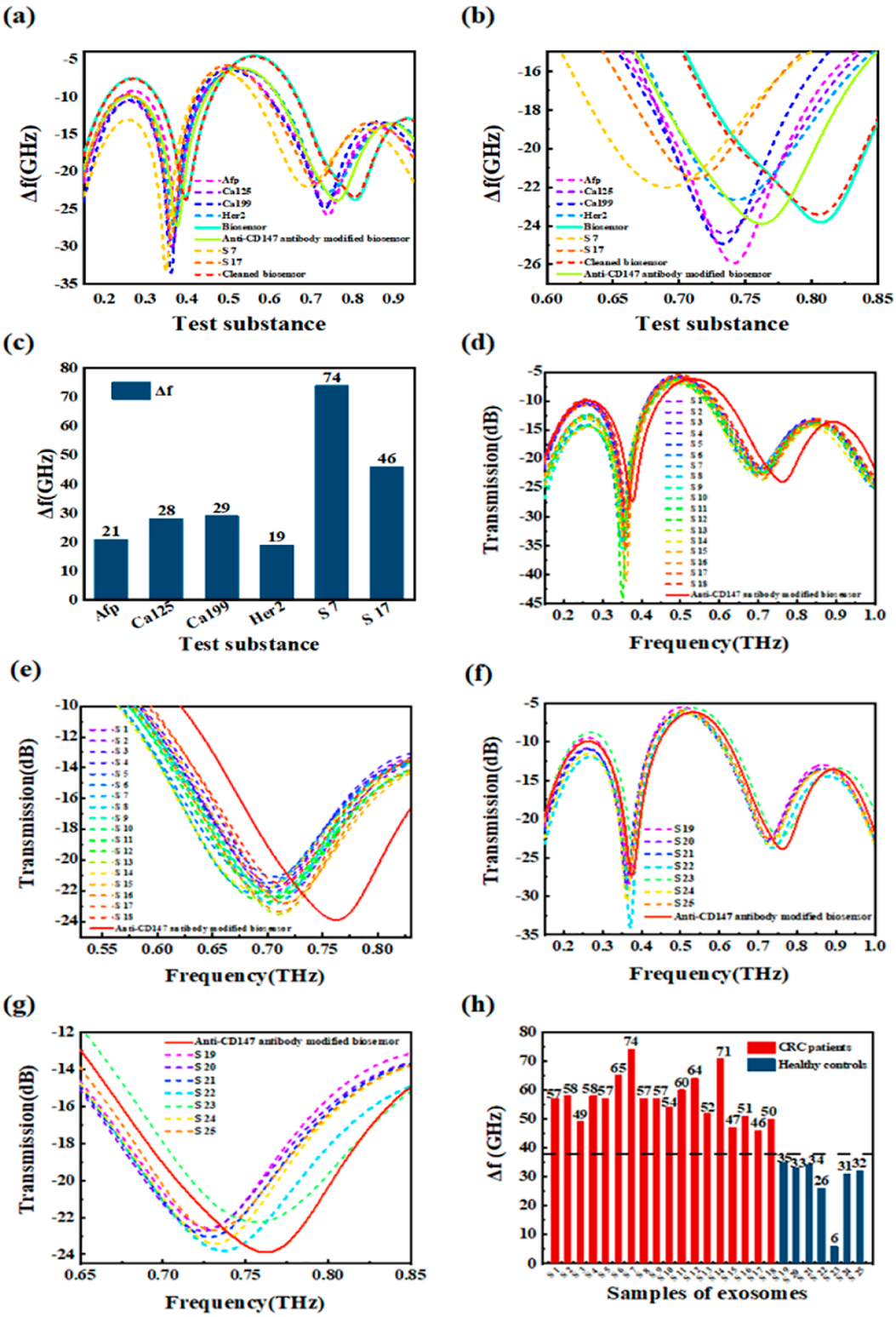


**Figure 7.** (a) Transmission spectrum of the modified anti-CD147 biosensor after dropping different test substances. (b) Magnified view of panel a. (c) Histogram of the resonance frequency shift with six test substances. (d) Transmission spectrum of exosome samples from patients with CRC and (f) healthy controls. (e) Magnified view of panel d. (g) Magnified view of panel f. (h) Histogram of the resonance frequency shift with CRC and healthy controls.

repeatability. To further test the specificity of the proposed modification-based biosensor, five different detectors are measured. It can be observed from Figure 7c that the components that form the transmission spectrum of the biosensor are red-shifted by 21, 28, 29, 19, 74, and 46 GHz, respectively.

In comparison experiments with other proteins (such as Ca125, Ca199, and Her2), the $p$ value is 0.018 after statistical



https://doi.org/10.1021/acs.langmuir.1c03286
Langmuir 2022, 38, 3739−3747

analysis. It is shown that the detection sensitivity of the anti-CD147-modified biosensor to other substances is lower than that of exosomes, which further illustrates the specificity of the biosensor. Thus, high specific sensing of exosomes can be achieved with THz spectroscopy of the anti-CD147-modified biosensor.

To test the proposed the anti-CD147-modified biosensor for detecting CRC, exosome samples from patients with CRC and healthy controls are measured. The measured transmission spectrum and corresponding resonance frequency shift results are shown in Figure 7h.

The detection results of exosome samples from patients with CRC has a resonance frequency shift of between 46 and 71 GHz. The detection results of exosome samples from healthy controls show that the resonance frequency shift is between 6 and 35 GHz. The accuracy of the THz system is 3 GHz. Therefore, on the basis of the modified THz MMs biosensor's ability to detect secretions from patients with CRC, the biosensor can distinguish between patients with CRC and healthy controls. Six groups of data were selected from the healthy group and the patient group for statistical analysis. The $p$ value is 0.0078, and the SD value is 18.6297.

## IV. CONCLUSIONS

In this work, we propose a method that uses a modified THz MMs biosensor to quickly detect the CRC. The biosensor has two resonance frequencies, and a high resonance frequency is very sensitive to changes in the surrounding environment. Therefore, it is used to characterize the reaction between the exosomes and the antibodies. By sequential modification with AuNPs, anti-KRAS, and anti-CD147, the biosensor has high sensitivity and specificity for the exosomes. On the basis of the resonance frequency shift caused by exosomes, it is easy to distinguish the patients with CRC from the healthy controls. This study demonstrated that plasma exosome detection may be effective for the repetitive and noninvasive diagnosis of patients with CRC, particularly in patients without the opportunity for a biopsy prior to treatment selection. The modified THz MMs biosensor has great potential in realizing modern clinical and pharmacological equipment with high sensitivity, high specificity, and repeatability.

## AUTHOR INFORMATION


### Corresponding Authors

**Fangrong Hu** − *Guangxi Key Laboratory of Optoelectronic Information Processing, Guilin University of Electronic Technology, Guilin 541004, China;* orcid.org/0000-0003-2835-1980; Phone: 86-0773-2290806; Email: hufangrong@sina.com, zlzh588@sohu.com

**Lizhen Zeng** − *Guangxi Key Laboratory of Optoelectronic Information Processing, Guilin University of Electronic Technology, Guilin 541004, China*; Email: yjsy@guet.edu.cn

### Authors

**Yao Wang** − *Guangxi Key Laboratory of Optoelectronic Information Processing, Guilin University of Electronic Technology, Guilin 541004, China*

**Yuanli Wang** − *Guangxi Key Laboratory of Optoelectronic Information Processing, Guilin University of Electronic Technology, Guilin 541004, China; Precision Medicine Laboratory, The First People's Hospital of Qinzhou, Qinzhou 535000, China*

**Zhencheng Chen** − *Guangxi Key Laboratory of Optoelectronic Information Processing, Guilin University of Electronic Technology, Guilin 541004, China*

**Mingzhu Jiang** − *Guangxi Key Laboratory of Optoelectronic Information Processing, Guilin University of Electronic Technology, Guilin 541004, China; Institute of Information Technology of Guilin, Guilin 541004, China*

**Shangjun Lin** − *Guangxi Key Laboratory of Optoelectronic Information Processing, Guilin University of Electronic Technology, Guilin 541004, China*

**Wei Guo** − *Guangxi Key Laboratory of Optoelectronic Information Processing, Guilin University of Electronic Technology, Guilin 541004, China*

**Dongxia Li** − *Guangxi Key Laboratory of Optoelectronic Information Processing, Guilin University of Electronic Technology, Guilin 541004, China*

Complete contact information is available at: https://pubs.acs.org/10.1021/acs.langmuir.1c03286


### Author Contributions

⊥Yuanli Wang is co-first author.

### Notes

The authors declare no competing financial interest.

## ACKNOWLEDGMENTS

This work is supported in part by the National Natural Science Foundation of China (62065005 and 62003107), the Natural Science Foundation of Guangxi, China (2018GXNSFAA050043, 2020GXNSFDA238019, and 2020GXNSFBA238012), the Key R & D project in Hunan Province (2020SK2111), the Foundation from Guangxi Key Laboratory of Automatic Detecting Technology and Instrument (YQ21101), the Innovation Project of Guangxi Graduate Education, China (2021YCXB06 and 19YJPYBS04), and the Health Commission of Guangxi Zhuang Autonomous Region (Z20200599).

## REFERENCES

(1) Bray, F.; Ferlay, J.; Soerjomataram, I.; et al. Global cancer statistics 2018: GLOBOCAN estimates of incidence and mortality worldwide for 36 cancers in 185 countries [J]. *CA: a cancer journal for clinicians* **2018**, *68* (6), 394−424.

(2) Conrad, S. J.; Essani, K. Oncoselectivity in Oncolytic Viruses against Colorectal Cancer [J]. *Journal of Cancer Therapy* **2014**, *5* (13), 1153−1174.

(3) Hofsli, E.; Sjursen, W.; Prestvik, W. S.; et al. Identification of serum microRNA profiles in colon cancer [J]. *Br. J. Cancer* **2013**, *108* (8), 1712−1719.

(4) Garborg, K.; Holme, O.; Lberg, M.; et al. Current status of screening for colorectal cancer [J]. *Annals of Oncology Official Journal of the European Society for Medical Oncology* **2013**, *24*, 1963−1972.

(5) Thanikachalam, K.; Khan, G. Colorectal Cancer and Nutrition [J]. *Nutrients* **2019**, *11* (1), 164.

(6) Farrell, N. P. Preclinical perspectives on the use of platinum compounds in cancer chemotherapy [J]. *Seminars in Oncology* **2004**, *31*, 1−9.

(7) Du, Y.; Wang, Y.; Hu, X.; et al. Single-molecule quantification of 5-methylcytosine and 5-hydroxymethylcytosine in cancer genome [J]. *View* **2020**, *1* (2), No. e9.

(8) Miccio, L.; Cimmino, F.; Kurelac, I.; et al. Perspectives on liquid biopsy for label-free detection of "circulating tumor cells" through intelligent lab-on-chips [J]. *View* **2020**, *1* (3), 20200034.

(9) Wan, J.; Pei, C.; Liu, C.; et al. FeOOH@Metal-Organic Framework Core-Satellite Nanocomposites for Serum Metabolic

Fingerprints of Gynecological Cancers [J]. *Angew. Chem.* **2020**, *132* (27), 10923−10927.
(10) Huang, L.; Wang, L.; Hu, X.; et al. Machine learning of serum metabolic patterns encodes early-stage lung adenocarcinoma [J]. *Nat. Commun.* **2020**, *11* (1), 3556.
(11) Su, H.; Li, X.; Huang, L.; et al. Plasmonic Alloys Reveal a Distinct Metabolic Phenotype of Early Gastric Cancer [J]. *Adv. Mater.* **2021**, *33* (17), No. 2007978.
(12) Li, X.; Kulkarni, A. S.; Liu, X. Metal-Organic Framework Hybrids Aid Metabolic Profiling for Colorectal Cancer [J]. *Small Methods* **2021**, *5*(4), DOI: 10.1002/smtd.202001001.
(13) Ladabaum, U.; Dominitz, J. A.; Kahi, C.; et al. Strategies for Colorectal Cancer Screening [J]. *Gastroenterology* **2020**, *158* (2), 418−432.
(14) Ma, Z.; Williams, M.; Cheng, Y. Y.; et al. Roles of Methylated DNA Biomarkers in Patients with Colorectal Cancer [J]. *Disease Markers* **2019**, *2019*, 1−8.
(15) Swiderska, M.; Barbara, C.; Ewelina, D.; et al. The diagnostics of colorectal cancer [J]. *Contemporary Oncology* **2014**, *18* (1), 1−6.
(16) Johnstone, R. M.; Adam, M.; Hammond, J. R.; et al. Vesicle formation during reticulocyte maturation. Association of plasma membrane activities with released vesicles (exosomes) [J]. *J. Biol. Chem.* **1987**, *262*, 9412−9420.
(17) Fearon, E. R. Molecular Genetics of Colorectal Cancer [J]. *Annual Review of Pathology: Mechanisms of Disease* **2011**, *6* (1), 479−507.
(18) Shang, A.; Gu, C.; Zhou, C.; et al. Exosomal KRAS mutation promotes the formation of tumor-associated neutrophil extracellular traps and causes deterioration of colorectal cancer by inducing IL-8 expression [J]. *Cell Communication and Signaling: CCS* **2020**, *18* (1), 52.
(19) Demory Beckler, M.; Higginbotham, J. N.; Franklin, J. L.; et al. Proteomic Analysis of Exosomes from Mutant KRAS Colon Cancer Cells Identifies Intercellular Transfer of Mutant KRAS [J]. *Molecular & Cellular Proteomics* **2013**, *12* (2), 343−355.
(20) Roock, W. D.; Vriendt, V. D.; Normanno, N.; et al. KRAS, BRAF, PIK3CA, and PTEN mutations: implications for targeted therapies in metastatic colorectal cancer [J]. *Lancet Oncology* **2011**, *12* (6), 594−603.
(21) Walther, A.; Johnstone, E.; Swanton, C.; et al. Genetic prognostic and predictive markers in colorectal cancer [J]. *Nature Reviews Cancer* **2011**, *11* (4), 309−309.
(22) Tian, Y.; Ma, L.; Gong, M.; et al. Protein Profiling and Sizing of Extracellular Vesicles from Colorectal Cancer Patients via Flow Cytometry [J]. *ACS Nano* **2018**, *12* (1), 671−680.
(23) Wang, L.; Deng, Y.; Huang, Y.; et al. Template-free multiple signal amplification for highly sensitive detection of cancer cell-derived exosomes [J]. *Chem. Commun.* **2021**, *57* (68), 8508−8511.
(24) Sun, Z.; Wang, L.; Wu, S.; et al. An Electrochemical Biosensor Designed by Using Zr-Based Metal Organic Frameworks for the Detection of Glioblastoma-Derived Exosomes with Practical Application [J]. *Anal. Chem.* **2020**, *92* (5), 3819−3826.
(25) Wang, L.; Pan, Y.; Liu, Y.; et al. Fabrication of an Aptamer-Coated Liposome Complex for the Detection and Profiling of Exosomes Based on Terminal Deoxynucleotidyl Transferase-Mediated Signal Amplification [J]. *ACS Appl. Mater. Interfaces* **2020**, *12* (1), 322−329.
(26) Pan, Y.; Wang, L.; Deng, Y.; et al. A simple and sensitive method for exosome detection based on steric hindrance-controlled signal amplification [J]. *Chem. Commun.* **2020**, *56* (89), 13768−13771.
(27) Wang, L.; Yang, Y.; Liu, Y.; et al. Bridging exosome and liposome through zirconium-phosphate coordination chemistry: a new method for exosome detection [J]. *Chem. Commun.* **2019**, *55* (18), 2708−2711.
(28) Wang, L.; Deng, Y.; Wei, J.; et al. Spherical nucleic acids-based cascade signal amplification for highly sensitive detection of exosomes [J]. *Biosens. Bioelectron.* **2021**, *191*, 113465.
(29) Wang, M. H.; Pan, Y. H.; Wu, S.; et al. Detection of colorectal cancer-derived exosomes based on covalent organic frameworks [J]. *Biosens. Bioelectron.* **2020**, *169*, 112638.
(30) Chen, H.; Chen, T. H.; Tseng, T. F.; et al. High-sensitivity in vivo THz transmission imaging of early human breast cancer in a subcutaneous xenograft mouse model [J]. *Opt. Express* **2011**, *19* (22), 21552−21562.
(31) Yu, L.; Hao, L.; Meiqiong, T.; et al. The medical application of terahertz technology in non-invasive detection of cells and tissues: opportunities and challenges [J]. *RSC Adv.* **2019**, *9* (17), 9354−9363.
(32) Hidayat, M. V.; Apriono, C. Simulation of Terahertz Imaging Using Microstrip Linear Array Antenna for Breast Cancer Detection [C]. *Second International Conference of Mathematics (SICME2019)*; 2019; Vol. *2092*, p 020020.
(33) Takida, Y.; Nawata, K.; Minamide, H. Security screening system based on terahertz-wave spectroscopic gas detection [J]. *Opt. Express* **2021**, *29* (2), 2529−2537.
(34) Tian, Y.; Ma, L.; Gong, M.; et al. Protein Profiling and Sizing of Extracellular Vesicles from Colorectal Cancer Patients via Flow Cytometry [J]. *ACS Nano* **2018**, *12* (1), 671−680.
(35) Woodward, R. M.; Cole, B. E.; Wallace, V. P.; et al. Terahertz pulse imaging in reflection geometry of human skin cancer and skin tissue [J]. *Physics in Medicine & Biology* **2002**, *47* (21), 3853−3863.
(36) Al-Naib, I. Biomedical Sensing wth Conductively Coupled Terahertz Metamaterial Resonators [J]. *IEEE J. Sel. Top. Quantum Electron.* **2017**, *23* (4), 1−5.
(37) Yan, X.; Yang, M. S.; Zhang, Z.; et al. The terahertz electromagnetically induced transparency-like metamaterials for sensitive biosensors in the detection of cancer cells [J]. *Biosens. Bioelectron.* **2019**, *126*, 485−492.
(38) Zhao, R.; Zou, B.; Zhang, G. L.; et al. High-sensitivity identification of aflatoxin B1 and B2 using terahertz time-domain spectroscopy and metamaterial-based terahertz biosensor [J]. *J. Phys. D: Appl. Phys.* **2020**, *53* (19), 195401.
(39) Li, B.; Zhao, X.; Zhang, Y.; et al. Prediction and monitoring of leaf water content in soybean plants using terahertz time-domain spectroscopy [J]. *Computers and Electronics in Agriculture* **2020**, *170* (2), 105239.
(40) Zhu, Z.; Cheng, C.; Chang, C.; et al. Characteristic fingerprint spectrum of neurotransmitter norepinephrine with broadband terahertz time-domain spectroscopy [J]. *Analyst* **2019**, *144* (8), 2504−2510.
(41) Chen, K.; Xu, D.; Li, J.; Geng, X.; Zhong, K.; Yao, J.; et al. Application of terahertz time-domain spectroscopy in atmospheric pressure plasma jet diagnosis - ScienceDirect [J]. *Results in Physics* **2020**, *16*, 102928.
(42) Frens, G. *Controlled Nucleation for the Regulation of the Particle Size in Monodisperse Gold Suspensions [M]*; Macmillan, 1973; Vol. *241*, pp 20−22.
(43) Xiao, Y. W.; Zhong, J. N.; Zhong, B. Y.; et al. Exosomes as potential sources of biomarkers in colorectal cancer [J]. *Cancer Letters* **2020**, *476*, 13−22.


https://doi.org/10.1021/acs.langmuir.1c03286
*Langmuir* 2022, 38, 3739−3747